

# Hormone-sensitive lipase is localized at synapses and is necessary for normal memory functioning in mice

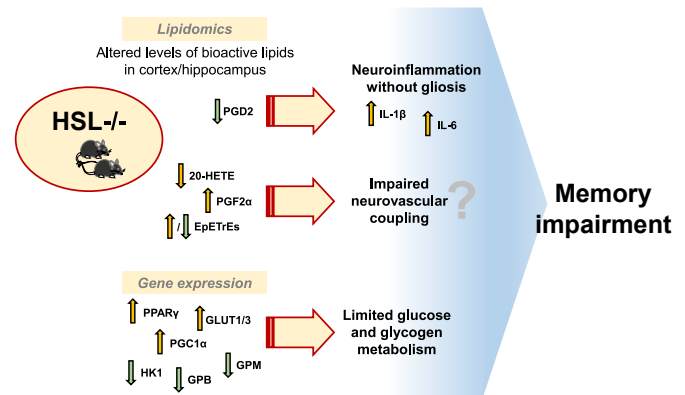
Cecilia Skoug<sup>1,2</sup> , Cecilia Holm<sup>1</sup>, and João M. N. Duarte<sup>1,2,\*</sup> 

<sup>1</sup>Department of Experimental Medical Science, and <sup>2</sup>Wallenberg Centre for Molecular Medicine, Faculty of Medicine, Lund University, Lund, Sweden

**Abstract** Hormone-sensitive lipase (HSL) is mainly present in adipose tissue where it hydrolyzes diacylglycerol. Although expression of HSL has also been reported in the brain, its presence in different cellular compartments is uncertain, and its role in regulating brain lipid metabolism remains hitherto unexplored. We hypothesized that HSL might play a role in regulating the availability of bioactive lipids necessary for neuronal function and therefore investigated whether dampening HSL activity could lead to brain dysfunction. In mice, we found HSL protein and enzymatic activity throughout the brain, localized within neurons and enriched in synapses. HSL-null mice were then analyzed using a battery of behavioral tests. Relative to wild-type littermates, HSL-null mice showed impaired short-term and long-term memory, yet preserved exploratory behaviors. Molecular analysis of the cortex and hippocampus showed increased expression of genes involved in glucose utilization in the hippocampus, but not cortex, of HSL-null mice compared with controls. Furthermore, lipidomics analyses indicated an impact of HSL deletion on the profile of bioactive lipids, including a decrease in endocannabinoids and eicosanoids that are known to modulate neuronal activity, cerebral blood flow, and inflammation processes. Accordingly, mild increases in the expression of proinflammatory cytokines in HSL mice compared with littermates were suggestive of low-grade inflammation. We conclude that HSL has a homeostatic role in maintaining pools of lipids required for normal brain function. **It remains to be tested, however, whether the recruitment of HSL for the synthesis of these lipids occurs during increased neuronal activity or whether HSL participates in neuroinflammatory responses.**

**Supplementary key words** endocannabinoids • eicosanoids • metabolism • inflammation • animal models • hippocampus • cortex • lipidomics • exploratory behavior • cerebral blood flow

Breakdown of triacylglycerols (TAGs) in adipose tissue is under hormonal regulation and is mediated by adipose triglyceride lipase that hydrolyzes a fatty acid from TAG-generating diacylglycerol (DAG), then the



hormone-sensitive lipase (HSL) hydrolyzes DAGs, and finally monoacylglycerol lipase (MAGL) degrades monoacylglycerols into a fatty acid and glycerol. HSL is abundant in the adipose tissues, where it mainly hydrolyzes DAG and plays a key role in lipolysis regulation since it is stimulated by catecholamines and inhibited by insulin (1).

The brain, like most organs, utilizes fatty acids as oxidative substrate (2, 3). The brain expresses adipose triglyceride lipase (4) and HSL (1), which have been suggested to control the release of free fatty acids to be used as energy substrate. Although brain cells can oxidize alternative substrates under a variety of physiological or pathological conditions, glucose is the obligatory fuel for adequate brain function (5, 6). Therefore, HSL is unlikely to be necessary for regulating fatty acid availability from acylglycerols for local energy production.

MAGL activity is ubiquitous in the brain and has a pivotal role in the endocannabinoid system: it terminates the action of the main endocannabinoid 2-arachidonoylglycerol (2-AG) through hydrolysis into glycerol and arachidonic acid (7). This is an example in which the lipase is not fulfilling energetic needs of brain cells but contributing to functional control of neuronal activity. Endocannabinoids control brain metabolism and synaptic function (8). The endocannabinoid 2-AG is synthesized by diacylglycerol lipase

\*For correspondence: João M. N. Duarte, [joao.duarte@med.lu.se](mailto:joao.duarte@med.lu.se).

(DAGL)  $\alpha$  and  $\beta$  at postsynaptic terminals following stimulation by glutamate and is then released to presynaptic terminals, where it stimulates cannabinoid 1 receptors, thus dampening glutamatergic activity at synapses (9). Moreover, cannabinoid 1 receptors directly inhibit mitochondrial metabolism in neurons and astrocytes (10), which may contribute to 2-AG-dependent synaptic control. Interestingly, while having negligible 2-AG hydrolysis activity (7), HSL could rather fulfill a role in hormone-regulated 2-AG production, thus integrating signaling from catecholamines and cannabinoids at neuronal synapses.

The main endocannabinoids 2-AG and *N*-arachidonylethanolamine (or anandamide) are quickly hydrolyzed by MAGL (11) and fatty acid amide hydrolase (FAAH) (12), respectively. These reactions produce arachidonic acid that, in turn, is enzymatically oxidized to produce eicosanoids that are proinflammatory mediators (13) and modulators of cerebral blood flow (5, 14). Thus, DAG hydrolysis by HSL could also contribute to regulate metabolic and signaling pools of arachidonic acid and other bioactive lipids.

Given the ability of HSL to be controlled by multiple cellular signals (15), we propose that its activity in the brain is poised to regulate lipid metabolism in cellular compartments where lipolysis is stimulated on demand for release of precursor fatty acids from esterified forms, which are then used for production of bioactive lipids. In this study, we aimed at mapping the relative distribution of HSL in the rodent brain and investigating the impact of HSL deletion on brain function, namely memory performance, and exploring underlying mechanisms.

## MATERIALS AND METHODS

### Animal models

All procedures on animals were approved by the Malmö-Lund Committee for Animal Experiment Ethics and conducted according to EU Directive 2010/63/EU and are reported following the ARRIVE guidelines (Animal Research: Reporting In Vivo Experiments, NC3Rs initiative, UK). Mice were housed on a 12-h light-dark cycle with lights on at 7:00, room temperature of 21–23°C and humidity at 55–60%, and had access to regular chow and water ad libitum. Male C57BL/6J mice were obtained from Taconic (Ry, Denmark) at 8 weeks of age and allowed to acclimatize to the animal facility for at least 2 weeks before experiments. HSL-null (HSL<sup>-/-</sup>) mice were generated by targeted disruption of the HSL gene (*Lipe*) in 129SV-derived embryonic stem cells as described elsewhere (16) and back-crossed to a C57BL/6J background for nine generations. HSL<sup>-/-</sup> mice and wild-type littermates (HSL<sup>+/+</sup>) of either gender were studied at 19–22 months of age.

### Neuronal cell cultures

Primary embryonic neurons were prepared from the cortices and hippocampi of embryonic day 15–17 WT mouse embryos, as detailed by Martinsson *et al.* (17). Briefly, neurons were dissociated through trypsinization and subsequent trituration in Dulbecco's modified Eagle's medium (catalog no.:

30243.01; Cytiva) supplemented with 10% fetal bovine serum (catalog no.: 10100-147; Gibco, Australia), 1% penicillin-streptomycin (catalog no.: 15140122; Thermo Fisher Scientific), and then placed onto poly-D-lysine-coated coverslips. After 3–5 h, medium was switched to Neurobasal medium supplemented with glutamine (catalog no.: 25030081; Thermo Fisher Scientific), B27 (catalog no.: A3582801; Thermo Fisher Scientific), and penicillin-streptomycin. Cells were grown in vitro for 19–20 days and then were fixed for 15 min in 4% paraformaldehyde and 4% sucrose at room temperature and stored in PBS (in mmol/l: 137 NaCl, 2.7 KCl, 1.5 KH<sub>2</sub>PO<sub>4</sub>, 8.1 Na<sub>2</sub>HPO<sub>4</sub>, pH 7.4) at 4°C until usage.

### Behavior testing

Mice were allowed to acclimatize to the testing room for 1 h before each experiment, and tests were performed from 9:00 to 18:00. Barnes maze tests were conducted under bright light over the platform. Otherwise, room light was adjusted to an illuminance of 15 lx in the test apparatus. Experiments were recorded by an infrared camera into the AnyMaze software (version 6.0.1; Stoelting).

A circular Barnes maze with diameter of 92 cm and 20 holes placed at a height of 90 cm was used to test learning and memory (18). The target hole had a removable dark escape box under the maze, and four proximal visual cues were placed at 20 cm from the platform. Experiments consisted of habituation, 8-day acquisition (training), and memory retention trial. For the habituation, mice were placed in the escape box during 60 s and then released in the center of the apparatus and allowed it to explore until re-entering the escape box or until 5 min elapsed. The first acquisition trial was conducted 2 h after the habituation and was used to probe short-term memory. Acquisition trials took place in 8 consecutive days, at the same time of the day, in which mice were released in the center of the maze with head pointing in random direction, and allowed to explore the maze for 5 min. The test ended when mice escaped into the target-hole box. Whenever mice did not find the escape box within 5 min, they were gently guided into it. The memory retention trial took place 48 h after the last acquisition session, under identical conditions but in the absence of any escape box. To eliminate olfactory cues, the surface and the escape box were cleaned with 70% (v/v) ethanol in-between each trial. Measured parameters were path and latency to reach or enter the target hole and time spent in each quadrant of the maze during retention trial (19).

Spontaneous alternations were observed in a Y-maze as surrogate of working memory performance (20). The Y-maze arms were 30 cm × 15 cm × 5 cm (length × height × wide) and converged to the center in 120° angles. Mice were placed an arm of the maze and allowed to freely explore for 5 min. A complete spontaneous alternation was defined as a successive entrance to each different arm and expressed relative to the total possible alternations in the respective test. The total number of entries was analyzed to access locomotor activity and exploratory behavior.

Open-field exploration was recorded for 5 min in a cubic arena with length of 50 cm by an infrared camera. Arena exploration was analyzed for total walk distance, number of crossings between arena quadrants and number of rearing events, as well as exploration of the arena center at 6 cm from the walls.

The elevated plus maze test was used to assess anxiety. Each maze arm was 35 cm × 5 cm, and closed arms had 15 cm walls, at a 60 cm height from the floor. The mouse was placed in the maze center facing an open arm and was allowed to freely

explore the maze for 5 min. Number of entries and time spent in each arm were analyzed (21).

### Tissue sampling

Mice were anesthetized with isoflurane and quickly decapitated, and brains were dissected, frozen in nitrogen (I), and stored at  $-80^{\circ}\text{C}$  until further experiments. For immunofluorescence experiments, mice under isoflurane anesthesia were sacrificed by cardiac perfusion with cold PBS and then cold phosphate-buffered formaldehyde (Histolab, Askim, Sweden), and brains were processed as detailed previously (22).

### Plasma glucose and insulin

A commercially available ELISA kit was used to determine plasma concentration of insulin (catalog no.: 10-1247-10; Mercodia, Sweden). Glucose plasma concentration was measured with glucose oxidase method using the substrate 2'-2-azino-bis(3-ethylbenzothiazoline-6-sulfonate) (catalog no.: 10102946001; Roche, Germany), and absorbance was measured at 420 nm (FLOUstar/Polystar Galaxy; BMG Labtech, Germany).

### HSL activity

Tissues were mechanically homogenized in 0.25 mol/l sucrose, 1 mmol/l EDTA, 1 mmol/l dithiothreitol, and protease inhibitors (20  $\mu\text{g}/\text{ml}$  leupeptin, 2  $\mu\text{g}/\text{ml}$  antipain, and 1  $\mu\text{g}/\text{ml}$  pepstatin), pH 7.0, using a glass-glass homogenizer. To remove fat from the tissues, it was centrifuged at 110,000  $g$  for 1 h at  $4^{\circ}\text{C}$  (Optima TLX Ultracentrifuge; Beckman), and the fat-free infranatant was used for HSL activity measurements. Measurement of HSL activity was performed using 1,3-oleoyl-2-0-oleylglycerol, a DAG analogue, as substrate, as previously detailed (23). It should be emphasized that the DAG analogue used as substrate does not generate substrate for MAGL because of the ether bond in position 2. To estimate the fraction of activity accounted for by HSL, samples were preincubated with either an activity-neutralizing hen antirat HSL serum (prepared in-house) or preimmune serum for 20 min at  $37^{\circ}\text{C}$  prior to the assay. Total protein content of the samples was measured with the bicinchoninic acid assay (kit from Pierce, Thermo Fisher Scientific; Göteborg, Sweden). Activity was expressed as mU/mg protein, where 1 U corresponds to the release of 1  $\mu\text{mol}$  of fatty acids per min at  $37^{\circ}\text{C}$ .

### Total protein extracts

Tissue samples were homogenized with a sonicator probe in lysis buffer (in mmol/l: 150 NaCl, 1 EDTA, 50 Tris(hydroxymethyl)aminomethane [Tris]-HCl, 1% [w/v] SDS, and pH 8.0) containing protease inhibitors (catalog no.: 11697498001; Roche, Switzerland) and phosphatase inhibitors (catalog no.: 4906837001; Roche, Switzerland). The homogenate was maintained in constant agitation for 2 h at  $4^{\circ}\text{C}$ . After centrifugation at 3,000  $g$  for 10 min at  $4^{\circ}\text{C}$  to remove major debris, the supernatant was saved. Protein concentration was determined as described previously.

### Preparation of synaptosomes and synaptic fractions

Synaptosomal fractionation was modified from the study by Morató *et al.* (24). Briefly, mouse cortex was homogenized in 1 ml of isolation buffer (in mmol/l: 320 sucrose, 0.1  $\text{CaCl}_2$ ,

0.1  $\text{MgCl}_2$ , and pH 7.4) at  $4^{\circ}\text{C}$  in a 5 ml Potter-Elvehjem glass/Teflon homogenizer (10 strokes at 700–900 rpm). The resulting homogenate was mixed with 6 ml sucrose (2 mol/l) and 2.5 ml  $\text{CaCl}_2$  (0.1 mmol/l) in an ultraclear centrifuge tube (catalog no.: 344059; Beckman Coulter). Then, 2.5 ml of sucrose (1 mol/l) containing 0.1 mM  $\text{CaCl}_2$  were carefully added on top to form a discontinuous sucrose gradient. All centrifugations were performed in an Optima XL-100K Ultracentrifuge (Beckman Coulter) with SW41Ti swinging bucket rotor (Beckman Coulter). After centrifugation for 3 h at 100,000  $g$ ,  $4^{\circ}\text{C}$ , the synaptosomes were collected from the interphase between 1.25 and 1 mol/l sucrose and diluted 10 times in isolation buffer, centrifuged for 30 min at 15,000  $g$ ,  $4^{\circ}\text{C}$ , and the resulting synaptosomal pellet was resuspended in 1 ml of isolation buffer.

For fractioning synaptosomes, part of each sample was diluted 1:5 in 0.1 mmol/l  $\text{CaCl}_2$ , and an equal volume of solubilization buffer (2% Triton X-100, 40 mmol/l Tris, pH 6.0) was added to the suspension. The suspension was incubated for 30 min on ice with constant agitation, and the insoluble material (synaptic junctions) was pelleted by centrifugation for 30 min at 40,000  $g$ ,  $4^{\circ}\text{C}$ . The supernatant (extrasynaptic fraction) was concentrated using an Amicon Ultra 15 10K (catalog no.: UFC901008; Merck Millipore, Ireland), and protein was precipitated with six volumes of acetone at  $-20^{\circ}\text{C}$  and recovered by centrifugation for 30 min at 18,000  $g$  at  $-15^{\circ}\text{C}$ . The pellet containing synaptic junctions was washed in solubilization buffer at pH 6.0 and then resuspended in 10 volumes of a second solubilization buffer (1% Triton X-100 and 20 mmol/l Tris, pH 8.0). After incubation under agitation for 30 min on ice, the mixture was centrifuged and the supernatant (presynaptic fraction) was processed as described for the extrasynaptic fraction, whereas the insoluble pellet corresponds to the postsynaptic fraction. All synaptic fractions were resuspended in 5% SDS with protease inhibitors.

### Immunoblotting

Western blotting was carried out as previously reported (25). Briefly, samples were heated for 5 min at  $95^{\circ}\text{C}$  in sample buffer (catalog no.: NP0007; Invitrogen) and then separated on 4–12% Bis-Tris mini gels (catalog no.: NP0336; Invitrogen), followed by transfer onto nitrocellulose membranes, pore size 0.45  $\mu\text{m}$  (catalog no.: GE10600002; GE Healthcare, Germany). The membranes were blocked for 60–120 min in 5% milk or bovine serum albumin in Tris-buffered saline (in mmol/l: 20 Tris, 150 NaCl, and pH 7.6) containing 1% Tween-20, and incubated with primary and secondary antibodies (Table 1) diluted in this blocking solution. Immunoblots were developed with a chemiluminescence kit (catalog no.: 34580; Thermo Fisher Scientific) using the Chemidoc XRS+ interfaced to Image Lab 5.2.1 for image analysis (Bio-Rad, Stockholm, Sweden).

### Immunofluorescence confocal microscopy

Primary neurons on cover glasses or 20  $\mu\text{m}$  cryostat-sectioned coronal brain slices were incubated for 1 h at room temperature with blocking buffer (PBS containing 5% [v/v] goat serum [catalog no.: 16210-064; Gibco, New Zealand], 1% [w/v] bovine serum albumin, and 0.3% [v/v] Triton X-100), followed by 2 h of incubation with primary antibodies (Table 1). After washing in PBS, the samples were incubated with AlexaFluor-conjugated secondary antibodies, washed again, mounted for microscopy with ProLong Glass Antifade



TABLE 1. Antibodies used for Western blotting (WB), activity assay (AA), and immunofluorescence microscopy (IF)

Antibody	Experiment	Source	Research Resource Identifier
Mouse monoclonal anti- $\beta$ -actin	WB	Sigma-Aldrich	AB_262011
Rabbit monoclonal anti-GFAP	WB	Abcam	AB_880202
Affinity-purified chicken anti-HSL	WB	In-house	AB_2892188
Rabbit polyclonal anti-Iba1	WB	FUJIFILM Wako	AB_839506
Rabbit anti-syntaxin 1	WB	Sigma-Aldrich	AB_261426
Rabbit monoclonal anti-syntaxin 4	WB	Abcam	AB_2891056
Rabbit monoclonal anti-SNAP25	WB	Abcam	AB_10887757
Rabbit monoclonal anti-synaptophysin	WB	Abcam	AB_2286949
Hen anti-rat HSL serum	AA	In-house	AB_2892189
Affinity-purified rabbit anti-HSL	IF	In-house	AB_2892190
Rabbit monoclonal anti-MAP2-Alexa 488 tagged	IF	Abcam	AB_2891057
Chicken polyclonal anti-MAP2	IF	Abcam	AB_2138153
Mouse monoclonal anti-NeuN	IF	Abcam	AB_10711040
Mouse monoclonal anti-PSD95	IF	Millipore	AB_2868387

Iba1, ionized calcium binding adapter molecule 1; MAP2, microtubule-associated protein 2.

(catalog no.: P36980; Invitrogen), and examined under a Nikon AIRHD confocal microscope with a CFI Apochromat TIRF 100 $\times$  Oil, numerical aperture 1.49 or CFI Plan Apochromat Lambda 20 $\times$ , numerical aperture 0.75 (Nikon Instruments, Tokyo, Japan). Images were acquired with NIS-elements (Laboratory Imaging, Nikon) and then processed in ImageJ (NIH, Bethesda, MD).

## RT-PCR

RNA was isolated from cortex and hippocampus from one hemisphere using Trizol (catalog no.: 15596026; Invitrogen) and then 1  $\mu$ g of total RNA was reverse transcribed with random hexamer primers using the qScript complementary DNA (cDNA) SuperMix (catalog no.: 95048; Quantabio, England), according to the manufacturers' instructions. The resulting cDNA was used as template for quantitative RT-PCR in triplicates using PerfeCTa SYBRgreen SuperMix (catalog no.: 95054; Quantabio, England) and the primers in [supplemental Table S1](#). Cycling and detection were carried out using Quantstudio 5 Real-time PCR system (40 cycles of 5 s at 95 $^{\circ}$ C and 30 s at 60 $^{\circ}$ C). Primers were optimized prior usage by assessing the optimal annealing temperature. Specificity was monitored using melt-curve validation and confirmation of amplified product by agarose gel electrophoresis. The dynamic range of each PCR assay was determined by constructing a standard curve using serial dilution of cDNA representative of each sample. Samples and standards were run in triplicate. All data were normalized to the expression of 60S ribosomal protein L14 and analyzed with the comparative threshold cycle method ( $\Delta\Delta$ CT).

## Targeted lipidomics

Analysis of oxylipins ([supplemental Table S2](#)) and endocannabinoids ([supplemental Table S3](#)) in tissue by UHPLC-QqQMSMS was carried out as detailed before (26). Briefly, 500  $\mu$ l methanol was added to  $\sim$ 20 mg of sample material. The sample was shaken with two tungsten beads at 30 Hz for 3 min in a mixer mill (MM 400; Retsch) whereupon the beads were removed. Samples were centrifuged at 2,125  $g$  for 10 min at 4 $^{\circ}$ C, and 450  $\mu$ l of the supernatant was diluted in 8.5 ml of 0.1% acetic acid to reduce the methanol concentration to  $\leq$ 5%. Blank samples, that is, samples without starting material, were prepared the same way as the tissue samples.

Solid-phase extraction was carried out on a Pressure+ 48 (positive pressure Manifold; Biotage) at  $\leq$ 2 psi. Solid-phase extraction columns were prewet with 1 ml methanol and

then equilibrated with 2 ml wash buffer (5% [v/v] methanol, 0.1% [v/v] acetic acid). Samples spiked with internal standard mixtures of endocannabinoids (20  $\mu$ l) and oxylipins (10  $\mu$ l) were added to the columns. After washing with 2 ml wash buffer, the samples were eluted with 3 ml acetonitrile, followed by 2 ml methanol. Finally, the samples were dried using a vacuum concentrator (miVac Quattro Concentrator; Genevac) and reconstituted in 110  $\mu$ l of 2.27  $\mu$ g/l 12-[[cyclohexylamino]carbonyl]amino]-dodecanoic acid in methanol.

Quantitative targeted liquid chromatography-mass spectrometry was conducted using an Agilent UHPLC system (Infinity 1290) coupled with an ESI to an Agilent 6490 triple quadrupole system equipped with iFunnel Technology (Agilent Technologies, Santa Clara, CA). Metabolite separation was performed using a Waters BEH C18 column (2.1 mm  $\times$  150 mm, 130  $\text{Å}$ , particle size of 1.7  $\mu$ m). The mobile phase consisted of (A) 0.1% acetic acid in Milli-Q water and (B) acetonitrile:isopropanol (90:10). A flow rate of 300  $\mu$ l/min and injection volumes of 10  $\mu$ l were employed for each run. The endocannabinoids are easily degraded compared with the relatively stable oxylipins, wherefore all samples were first injected for ionization in positive mode (endocannabinoids) followed by all samples injected for negative (oxylipins) mode.

Quantification of the compounds was performed with MassHunter Quantitative Analysis QQQ (Agilent). Analytes were quantified against native standards, with correction for recovery rates of deuterated internal standards, as detailed previously (26).

## Statistical analyses

Results were analyzed with Prism 9.0.2 (GraphPad Software, Inc, San Diego, CA). The Kolmogorov-Smirnov test was used for normality testing. In the absence of normality deviations, results were analyzed using unpaired, 2-tailed Students  $t$ -test or ANOVA followed by independent comparisons with the Fisher's least significant difference test. Significance was accepted for  $P < 0.05$ . Partial least-squares discriminant analysis (PLS-DA) with two components was applied on z-scores of gene expression or lipidomics datasets using MATLAB 2019a (MathWorks, Natick, MA). For that, each sample was assigned a dummy variable as a reference value (0 = HSL $^{-/-}$  and 1 = HSL $^{+/+}$ ). The variable importance in projection (VIP) was calculated for each gene or lipid in either brain area. Results are presented as mean  $\pm$  SD unless otherwise stated. Statistical details of experiments can be found in the figure legends.

## RESULTS

### HSL is enriched in neuronal synapses and is widely distributed in the brain

From the mouse cortex, we prepared synaptosomes, which are resealed nerve terminals after tissue homogenization. Synaptosomes were subsequently fractionated into synaptic preparations that are rich in postsynaptic density protein 95, synaptosomal-associated protein 25 (SNAP25), and synaptophysin, which correspond to the postsynaptic, presynaptic, and extrasynaptic zones, respectively (Fig. 1A). Upon immunoblotting, we observed two bands at the approximate molecular weight of previously described HSL isoforms (27), but only the band corresponding to the predominant isoform in adipose tissue (84 kDa) was absent from in protein extracts from HSL<sup>-/-</sup> mice (Fig. 1B). The synaptic fractions showed a more intense immunoreactivity against HSL than total protein extracts (Fig. 1B). Indeed, synaptosomes showed 8-fold more immunoreactivity than total extracts ( $P < 0.01$ ) and, among the synaptic preparations, HSL immunoreactivity was observed in presynaptic and mostly postsynaptic fractions (Fig. 1C). We then set to investigate the cerebral distribution of HSL. First, we measured DAG lipase activity in the absence or the presence of an anti-HSL antibody that abrogates HSL activity. Although HSL-specific DAG lipase activity was 20-fold lower in brain than in adipose tissue, it was detected in all brain areas analyzed, and on average, it accounted for about two-thirds of total DAG lipase activity (Fig. 1D). Then, the presence of HSL in these mouse brain samples was confirmed by immunoblotting experiments (Fig. 1E). Different unspecific bands in blots of Fig. 1B and E are attributed to difference in sample preparation.

Immunofluorescence microscopy in mouse brain slices showed that HSL immunoreactivity is observed within all cells that are positive for the widely used neuronal marker NeuN, as well as in NeuN-negative cells (Fig. 1F), suggesting that both neurons and glia express HSL. Notably, brain slices from HSL<sup>-/-</sup> mice showed no HSL immunoreactivity (Fig. 1G). In cultured cortical neurons, HSL immunoreactivity was observed in the cell soma and along dendritic processes (Fig. 2A). In finer dendrites, HSL immunoreactivity was adjacent to that of postsynaptic density protein 95 (Fig. 2B), in line with its synaptic location.

### Characteristics of HSL<sup>-/-</sup> mice

Mice in this study were 19–22 months old, and HSL<sup>-/-</sup> mice showed slightly lower body weight ( $29.6 \pm 4.9$  vs.  $36.7 \pm 6.6$  g,  $P < 0.05$ ), higher fed plasma insulin ( $1,874 \pm 1,005$  vs.  $701 \pm 782$  pmol/l,  $P < 0.01$ ) but similar plasma glucose ( $10.0 \pm 1.3$  vs.  $10.8 \pm 2.1$  mmol/l,  $P < 0.05$ ) compared with the corresponding wild-type littermates.

### HSL<sup>-/-</sup> mice display short-term and long-term memory impairment

To investigate whether HSL contributes to brain function, HSL<sup>-/-</sup> mice and wild-type littermates were analyzed using a battery of behavior tests that probe for memory, exploratory behavior and locomotor activity, and anxiety-like behavior.

Spatial learning and memory was analyzed using the Barnes maze, in which mice were trained for 8 days to learn the escape box location, that is the target hole, and long-term memory was analyzed after 48 h (Fig. 3A). Learning during the 8 training days was indistinct between genotypes (Fig. 3B). In training day 1, the experiment was preceded by a habituation session in which mice were placed in the escape whole, that is, the target, and released in the center of the arena 2 h later. Thereafter, the first training session revealed short-term memory impairment in HSL<sup>-/-</sup> mice, as depicted by larger latency ( $P < 0.05$ ) and number of errors until the target was reached ( $P < 0.05$ ), when compared with wild-type mice (Fig. 3C). During a training period of 8 days, HSL<sup>-/-</sup> mice utilized more often a random than serial hole search to identify the target (Fig. 3D). Long-term memory was probed 48 h later, with mice being allowed to explore the maze without the escape box. HSL<sup>-/-</sup> mice searched less holes in the target quadrant ( $P < 0.05$ ), took longer time to reach the target hole for the first time ( $P < 0.05$ ), and spent overall less time in the target quadrant than controls ( $P < 0.01$ , Fig. 3E), suggesting impaired spatial memory performance. The reduced Y-maze spontaneous alternation in HSL<sup>-/-</sup> mice compared with controls ( $P < 0.05$ ) further confirmed memory impairment caused by genetic HSL deletion (Fig. 3F).

These memory assessments were not biased by alterations of exploratory behavior since the genotype had no effect on the number of entries in the Y-maze arms (Fig. 3F), or on any measure of the open-field exploration, such as quadrant crossings, rearing, and total walked distance in the arena (Fig. 3G). HSL deletion was also unrelated to development of anxiety-like behaviors depicted by changes in the exploration of the unprotected open-field arena center (Fig. 1G) or of the open arms in the elevated plus maze test (Fig. 3H).

### HSL deletion impacts genes involved in glucose metabolism and inflammation

As a first step to investigate the impact of HSL deletion on brain metabolism, we measured the expression of a panel of genes coding for proteins involved in glucose and lipid metabolism and genes encoding enzymes involved in the endocannabinoid system. Since neuroinflammation is known to be involved in a number of neurological and metabolic disorders (28), this gene panel also included the master regulator of inflammatory processes NF- $\kappa$ B and

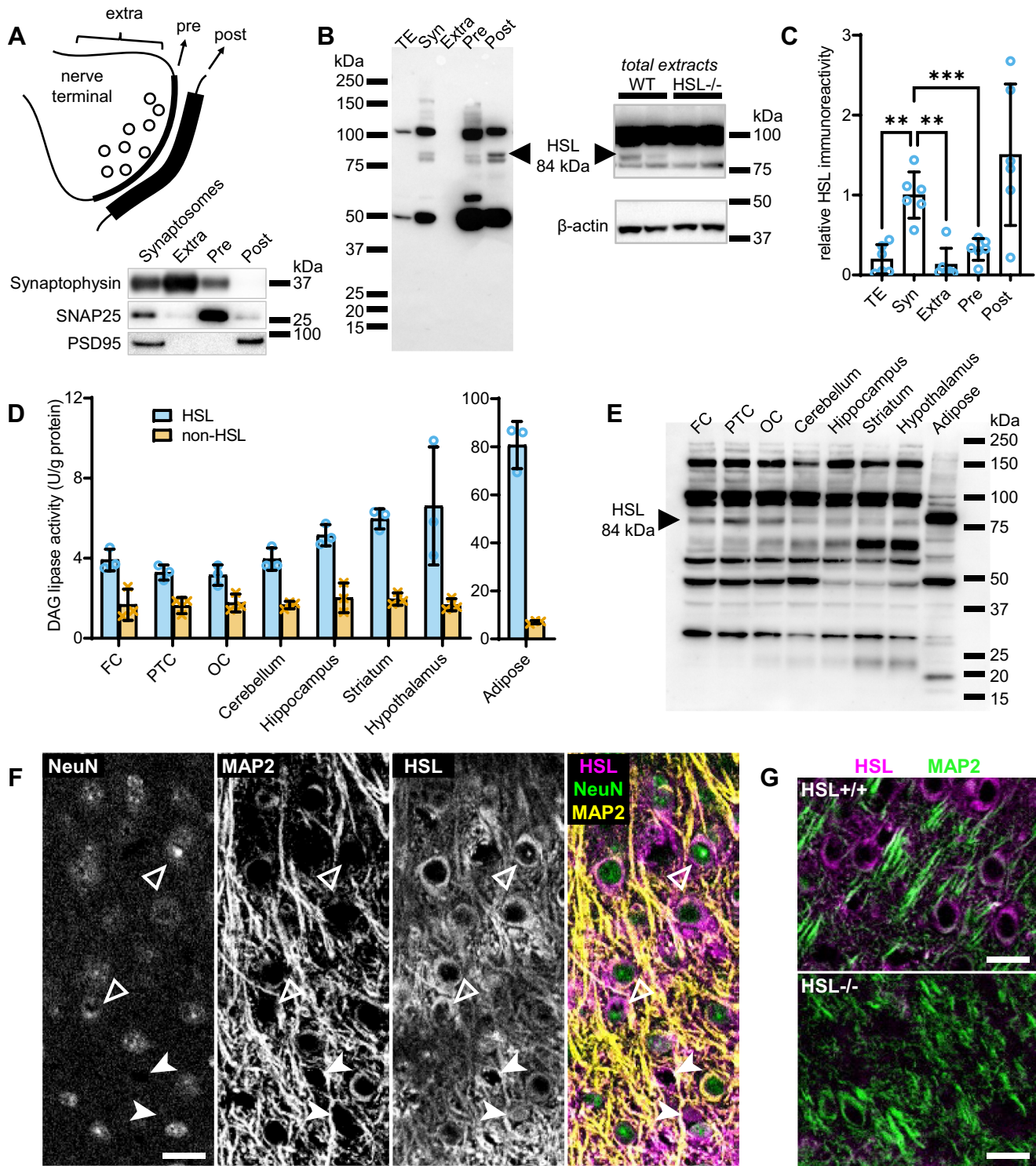


**Fig. 1.** HSL is present in neurons and distributed throughout the mouse brain. **A:** Western blots of presynaptic (Pre), postsynaptic (Post), and extrasynaptic (Extra) fractions prepared from the mouse cortex show enrichment in SNAP25, PSD95, and synaptophysin, respectively. **B:** Relative to total protein extracts (TE), synaptosomes, presynaptic and postsynaptic fractions show immunoreactivity against HSL, a band of 84 kDa that is absent from protein extracts of the HSL<sup>-/-</sup> mouse cortex (picture on the right). Protein loaded in gels was 30  $\mu$ g for comparison of synaptic fractions and TE, and 40  $\mu$ g for comparing TE from HSL<sup>-/-</sup> and wild-type (WT) littermates. **C:** Quantitative analysis of Western blot immunoreactivity suggests presynaptic and mostly postsynaptic HSL enrichment. **D** and **E:** HSL-specific (blue circles) and nonspecific (orange crosses) DAG lipase activity in brain areas and adipose tissue (**D**) and respective immunoreactivity in Western blotting (**E**). Protein loaded for immunoblotting was 40  $\mu$ g for brain samples and 15  $\mu$ g for adipose tissue. **F:** Representative fluorescence micrographs of the mouse brain cortex immunolabeled for HSL (magenta), NeuN (green), and MAP2 (yellow). HSL immunoreactivity appears within NeuN-positive (filled arrowhead) and NeuN-negative (open arrowhead) cells. **G:** The absence of immunoreactivity in cortical slices from HSL<sup>-/-</sup> mice. The scale bars in micrographs are 20  $\mu$ m. Data in bar graphs are represented as individual data points and mean  $\pm$  SD of  $n = 6$  in **C** and  $n = 3$  in **D**. Symbols over data points



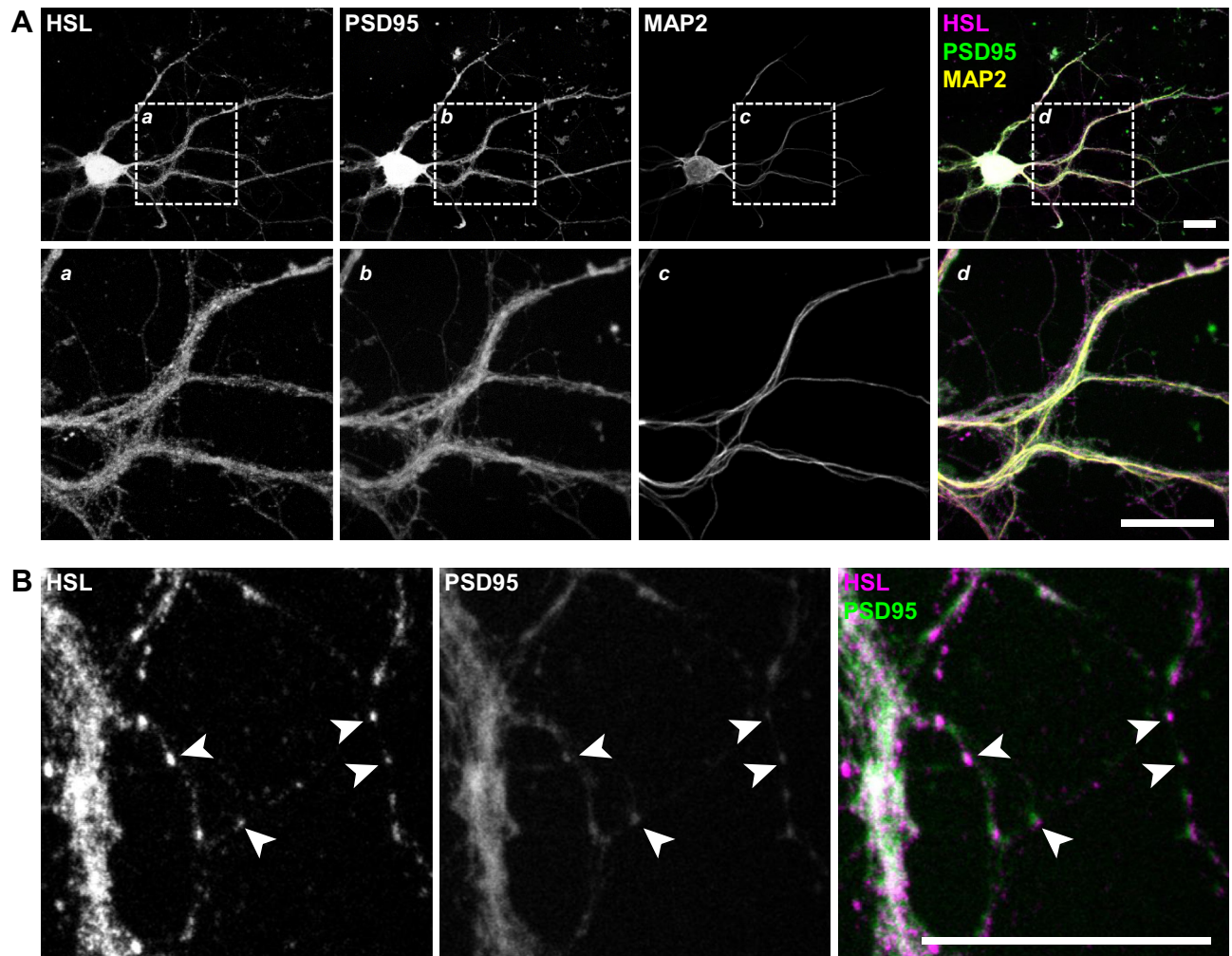


**Fig. 2.** HSL is observed in primary cultured neurons. **A:** Representative immunofluorescence micrographs of cultured cortical neurons stained for HSL (magenta), PSD95 (green), and MAP2 (yellow) showing HSL immunoreactivity throughout the cell soma and axons. **B:** Higher magnification images show adjacent immunoreactivity against HSL and PSD95 in fine neuronal processes (arrowheads). The scale bars in micrographs represent 20  $\mu\text{m}$ . MAP2, microtubule-associated protein 2; PSD95, postsynaptic density protein 95.

cytokines. Transcriptomics data from the hippocampus and cortex ([supplemental Fig. S1](#)) were analyzed with a two-component PLS-DA and allowed good separation of  $\text{HSL}^{-/-}$  and wild-type mice ([Fig. 4A](#)), with principal component 1 and principal component 2 accounting for 72% and 16% of the variance in gene expression. The VIPs calculated from the PLS-DA model coefficients ([Fig. 4B](#)) indicate that, in the hippocampus, HSL deletion increases the expression of genes necessary for glucose metabolism, namely those coding for the glucose carriers glucose transporter (GLUT)1 and GLUT3, the glycogen phosphorylase muscle isoform, as well as PPAR $\gamma$  and PPAR gamma coactivator 1 $\alpha$  (PGC1 $\alpha$ ) that are key in mitochondria physiology. The hippocampus of  $\text{HSL}^{-/-}$  mice also showed reduced expression of hexokinase 1 and a number of genes

coding for proteins involved in lipid metabolism (DAGL $\alpha$ , alpha/beta-hydrolase domain containing 6 [ABHD6], and MAGL). Some of these observations were paralleled in the cortex ([Fig. 4B](#)). However, most strikingly, the cortex showed a prominent increase of the proinflammatory interleukins IL-6 and IL-1 $\beta$  (IL-1 $\beta$  was also increased in hippocampus), suggesting the occurrence of neuroinflammation. Relative to wild-type littermates,  $\text{HSL}^{-/-}$  mice showed reduced expression of the gene coding for cyclooxygenase 1 (COX1) in the cortex, suggesting altered synthesis of eicosanoids that modulate inflammation. Given the association of HSL deletion to neuroinflammation, we then tested whether this process is accompanied by gliosis. Immunoblotting against the astrocytic marker glial fibrillary acidic protein (GFAP) or the microglial marker ionized

indicate significant differences between control and  $\text{HSL}^{-/-}$  mice (\*\* $P < 0.01$  and \*\*\* $P < 0.001$ ) based on Fisher's least significant difference post hoc comparison after ANOVA. FC, frontal cortex; MAP2, microtubule-associated protein 2; OC, occipital cortex; PSD95, postsynaptic density protein 95; PTC, parietotemporal cortex.

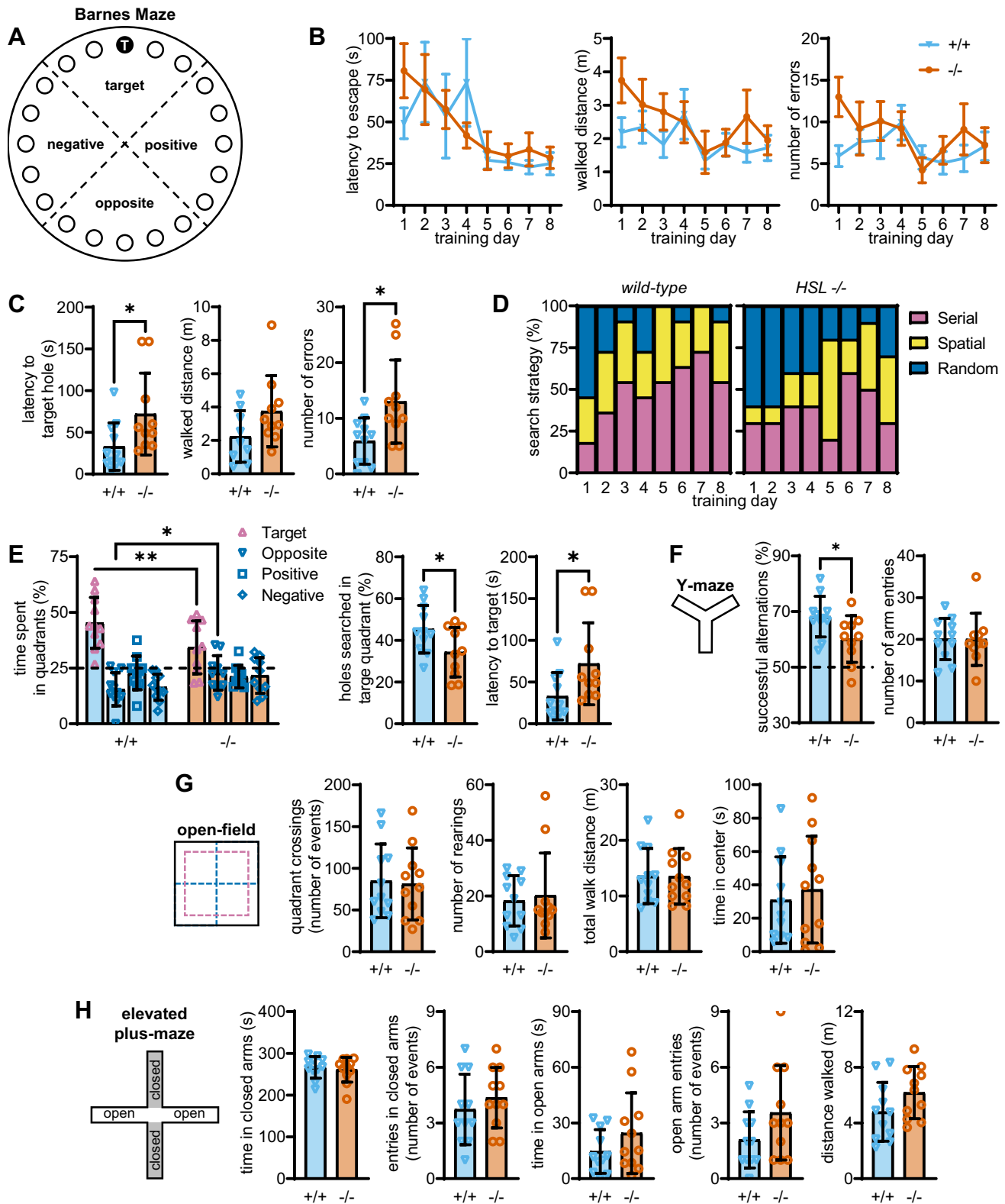


**Fig. 3.** HSL<sup>-/-</sup> mice show memory impairment while exploratory and anxiety-like behaviors are preserved. **A:** Schematic representation of the Barnes maze with holes numbered 1 to 10 from the target hole (T) and divided in four quadrants. **B:** Learning to find the target hole over the 8 acquisition days was not affected by genotype. **C:** Training in acquisition day 1 was followed after habituation to the maze and allowed to identify increased latency and walked distance until entering the target hole, an increased number of errors (nontarget hole searches) in HSL<sup>-/-</sup> versus wild-type mice. **D:** Compared with controls, HSL<sup>-/-</sup> mice utilized more often a random than serial hole search during the 8-day training period. **E:** Relative to controls, HSL<sup>-/-</sup> mice searched less holes in the target quadrant, took longer time to reach the target hole for the first time, and spent overall less time in the target quadrant during the probe session. Dashed line at 25% represents random exploration (chance). **F:** Fraction of successful spontaneous alternations (consecutive entries in the three arms) in the Y-maze was lower in HSL<sup>-/-</sup> mice than controls, while showing similar number



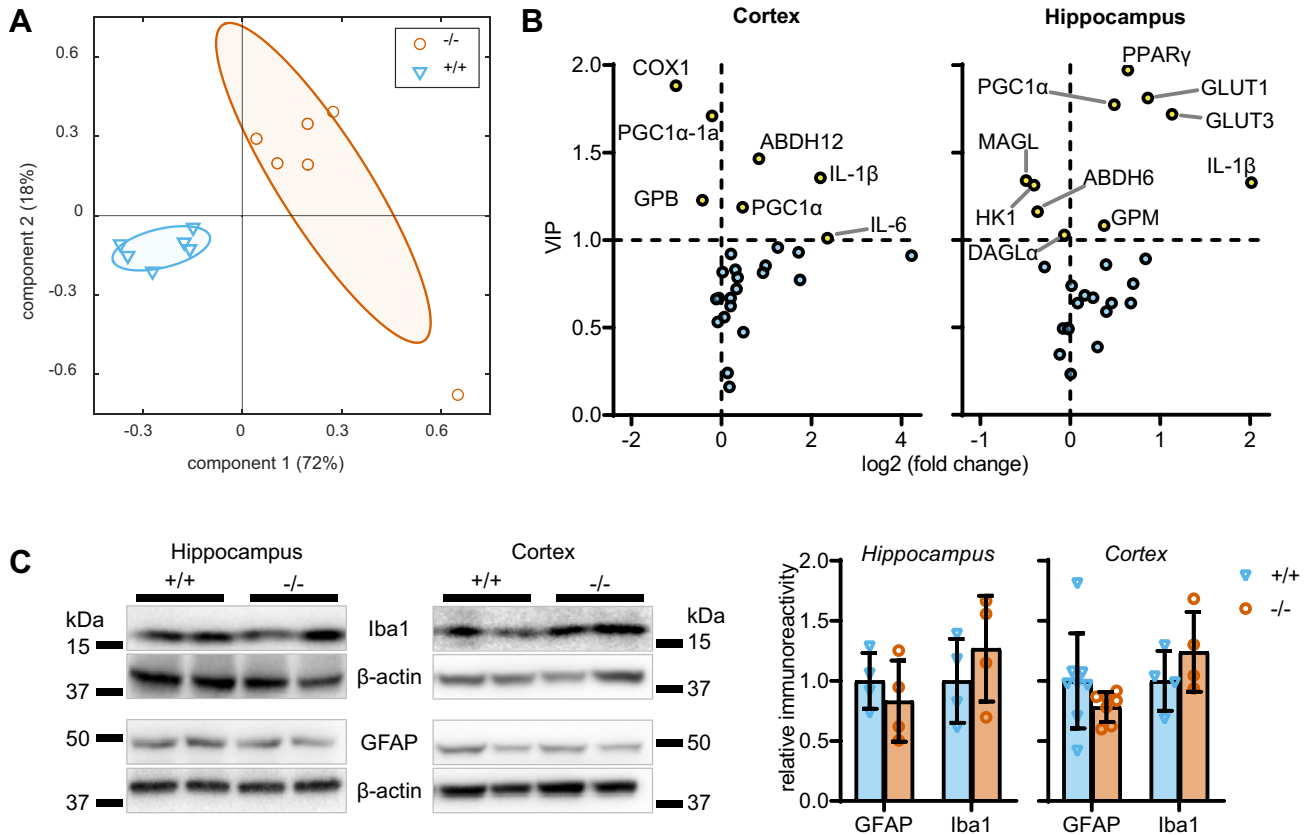


**Fig. 4.** Effect of HSL deletion on cortical and hippocampal expression of genes involved in inflammation and metabolism. A: Transcriptomics on 12 mice ( $n = 6/\text{genotype}$ ) revealed distinct gene expression between  $\text{HSL}^{+/+}$  and  $\text{HSL}^{-/-}$  mice in a PLS-DA, with PC1 and PC2 accounting for 72% and 16% of the total variance. Ellipsoids delineate SD. B: Volcano plots showing VIP for the PLS regression versus fold change in expression in the hippocampus and cortex. Proteins coded by genes with  $\text{VIP} > 1$  are labeled and highlighted in yellow. C: Relative immunoreactivity of the microglial marker ionized calcium binding adapter molecule 1 and astrocytic marker GFAP in total protein extracts of the cortex and hippocampus ( $n = 4-6$ ). Immunoreactivity is normalized to the average of controls. Data are represented as individual data points and mean  $\pm$  SD in bar graphs. PC1, principal component 1; PC2, principal component 2.

calcium binding adapter molecule 1 (allograft inflammatory factor 1) showed similar immunoreactivity in cortical or hippocampal extracts from  $\text{HSL}^{-/-}$  and  $\text{HSL}^{+/+}$  mice (Fig. 4C). Altogether, these results suggest that HSL deletion is associated with altered metabolism and low-grade neuroinflammation without the occurrence of important astrogliosis or microgliosis.

### HSL deletion does not impact typical markers of synaptic health

Since HSL is located in synapses, we then tested whether memory impairment upon HSL deletion was caused by loss of synaptic proteins involved in neurotransmitter release, as observed in various models of metabolic disease (29). Protein extracts from the cortex

showed reduced immunoreactivity against syntaxin-4 in  $\text{HSL}^{-/-}$  mice compared with controls ( $P < 0.05$ ), without substantial effects on syntaxin-1, SNAP25, or synaptophysin (Fig. 5A). In the hippocampus, the density of these four proteins was similar in the two genotypes (Fig. 5B).

### HSL deletion causes a shift in the profile of available bioactive lipids

Given the particular synaptic enrichment of HSL in synapses, it is plausible that cellular signaling through HSL is involved in the control of lipid metabolites that modulate synaptic physiology. Thus, in a further set of experiments, we determined the concentration of endocannabinoids and oxylipins in the hippocampus

of entries in the maze arms. Dashed line at 0.5 represents random arm entries. G: Genotype had no effect on open-field exploration, with similar number of quadrant crossings, rearing events (vertical explorations), walked distance in the arena, and time spent in the arena center. H: Elevated plus maze test showed no effect of genotype on either time spent and number of entries in closed and open arms or total distance walked in the maze. Data are represented as mean  $\pm$  SEM in line graphs of  $n = 10-11$  and as individual data points and mean  $\pm$  SD in bar graphs. Symbols over data points indicate significant differences between control and  $\text{HSL}^{-/-}$  mice ( $*P < 0.05$  and  $**P < 0.01$ ) based on Student's  $t$ -tests or Fisher's least significant difference post hoc comparison test following the presence of significant effects of genotype in ANOVA tests.

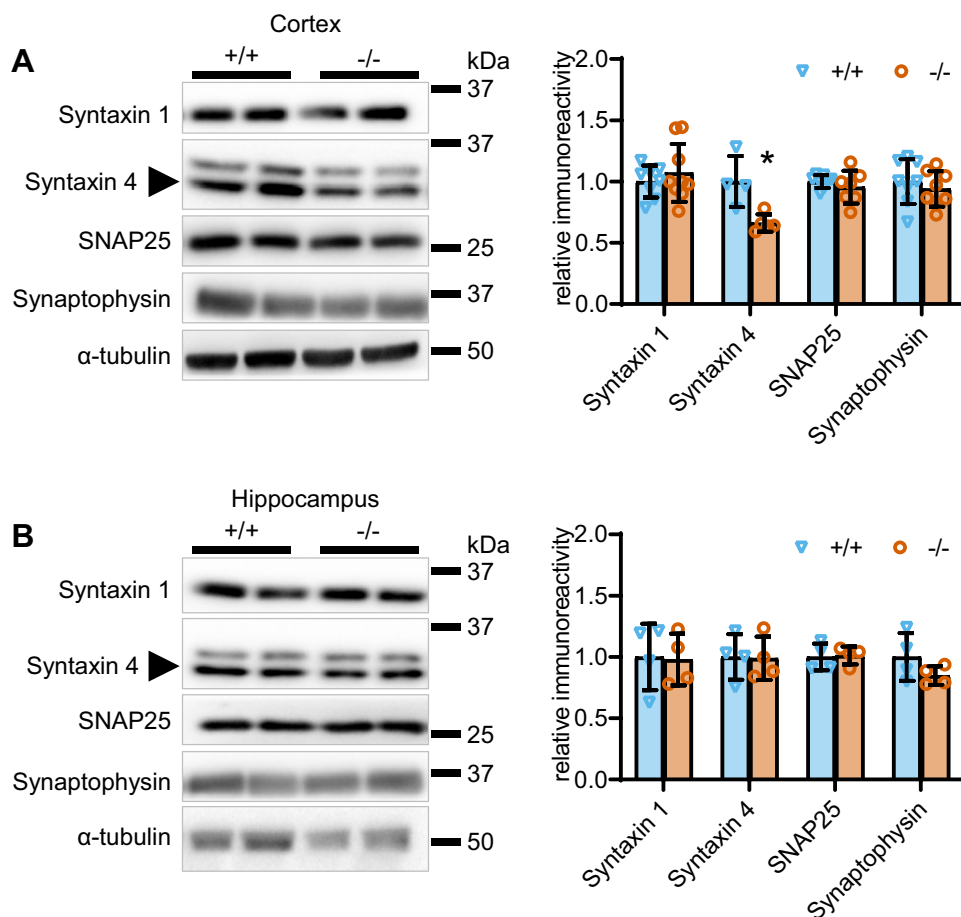


**Fig. 5.** Effect of HSL deletion on protein markers of synaptic health. Relative immunoreactivity of syntaxin-1 (35 kDa), syntaxin-4 (34 kDa; arrow), SNAP25 (25 kDa), and synaptophysin (37 kDa), which are key proteins involved in neurotransmitter release, in total protein extracts of the cortex (A) and hippocampus (B). Immunoreactivity is normalized to the average of controls. Data are represented as individual data points and mean  $\pm$  SD of  $n = 4-8$  in bar graphs. Symbols over data points indicate significant differences between control and HSL<sup>-/-</sup> mice (\* $P < 0.05$ ) based on two-tailed Student's *t*-tests.

and cortex. A panel of over 50 bioactive lipids was analyzed by mass spectrometry (supplemental Tables S2 and S3), and we then applied a two-component PLS-DA to determine the most important set of metabolites differentiating between HSL<sup>+/+</sup> and HSL<sup>-/-</sup> mice. We were able to observe a reasonable separation of the two genotypes (Fig. 6A), with principal component 1 and principal component 2 accounting for 32% and 36% of the variance in lipids. VIPs from the PLS-DA model coefficients allowed us to identify a number of bioactive lipids of importance in the genotype discrimination (Fig. 6B and C), including the endocannabinoids 2-linoleoylglycerol, *N*-arachidonoylglycine, palmitoleylethanolamide (POEA), anandamide, and docosahexaenoylethanolamide, the prostaglandins D2 (PGD2) and F2 $\alpha$  (PGF2 $\alpha$ ), and other eicosanoids such as 20-hydroxyarachidonic acid, the epoxyeicosatrienoic acids 5,6-EpETrE, 8,9-EpETrE, 11,12-EpETrE, and 14,15-EpETrE, among others. When analyzing concentrations of the lipids individually (supplemental Tables S2 and S3), however, no significant differences were observed between HSL<sup>-/-</sup> mice and littermates.

## DISCUSSION

Our results indicate that HSL is active throughout the brain and accounts for at least two-thirds of total DAG lipase activity throughout the assessed brain areas. Accordingly, HSL<sup>-/-</sup> mice were reported to have a substantial dampening of brain DAG lipase activity (1). It should be noted that our HSL activity assay is optimized for measuring HSL. It might be that the relative DAG lipase activity accounted from HSL is lower in the native tissue, which allows for further on-demand activation. Similarly, Blankman *et al.* (7) have assayed lipase activity under conditions that are far from optimal for HSL, and concluded that HSL has negligible 2-AG hydrolysis activity. Therefore, further studies are necessary for the determination of the exact roles of brain HSL.

Furthermore, the present study suggests that HSL is particularly located in synapses, where it might exert important regulatory mechanisms that are hitherto undescribed. For the first time, to our knowledge, we demonstrate here that HSL is necessary for memory performance, since the HSL<sup>-/-</sup> mouse exhibited

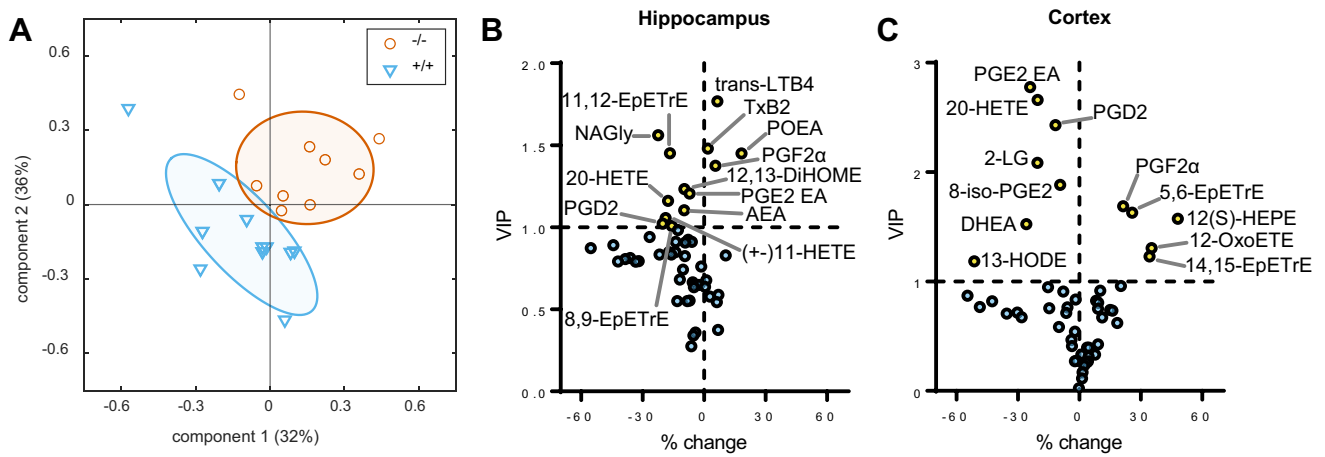


**Fig. 6.** Effect of HSL deletion on bioactive lipids. A: A panel of bioactive lipids analyzed by targeted mass spectrometry allowed to discriminate between HSL<sup>+/+</sup> and HSL<sup>-/-</sup> mice in a PLS-DA (six males and five females for HSL<sup>+/+</sup>; two males and seven females for HSL<sup>-/-</sup>). PC1 and PC2 accounted for 32% and 36% of the total variance. Ellipsoids represent SD. B and C: Volcano plots showing VIP for the PLS regression versus relative change in HSL<sup>-/-</sup> versus HSL<sup>+/+</sup>. Lipids in the hippocampus (B) and cortex (C) with VIP >1 are labeled and highlighted in yellow. For complete metabolite abbreviations and concentrations, see [supplemental Tables S2 and S3](#). PC1, principal component 1; PC2, principal component 2.

impaired short-term and long-term memory in the Barnes maze as well as impaired spatial working memory in the Y-maze. This role of HSL in cognition adds up to previous suggestions of HSL-mediated lipolysis modulating hypothalamic function (30, 31).

Given the synaptic enrichment of HSL, we evaluated whether degeneration of cortical and hippocampal synapses was a possible cause for memory impairment, as in other models of metabolic and neurological disorders (17, 29). Levels of synaptophysin, syntaxin-1, or SNAP25, which are enriched in nerve terminals, were not modified by HSL deletion. HSL deletion caused a reduction of syntaxin-4 levels in the cortex (but not hippocampus). Although this protein is part of the exocytosis machinery of nerve terminals, it is mainly present in processes of astrocytes (32). Therefore, it is possible that release of molecules from astrocytes acting on synapses is impaired. Nevertheless, we have not observed alterations in the levels of GFAP that is specific to astrocytes. Neuronal communication at synapses is crucial for cognition, and damage to synapses and impaired synaptic functions is associated to cognitive decline (33, 34). Although HSL<sup>-/-</sup> mice do not show loss of synaptic markers that is typical of neurodegeneration, one cannot exclude impairment in the modulation of neurotransmitter release.

Neuroinflammation is a key process by which lipid metabolism disorders and obesity impact brain function (28). HSL<sup>-/-</sup> mice show low-grade neuroinflammation characterized by higher expression of proinflammatory cytokines than wild-type littermates. This occurs mainly in the hippocampus and thus might contribute to the observed spatial memory impairment. Immunofluorescence experiments revealed HSL expression in NeuN-negative cells, which are likely

astrocytes or microglia. Moreover, the concentration of oxylipins involved in inflammatory processes was modified upon genetic HSL deletion (see later). Low-grade inflammation in adipose tissue of HSL<sup>-/-</sup> mice has been described (35). It has also been shown that HSL deficiency alters the expression of elongases and desaturases in liver and adipose tissue (36, 37), which might impact lipogenesis and the profile of circulating long-chain polyunsaturated fatty acids from which inflammatory mediators are synthesized. Therefore, given the pivotal participation of lipid metabolism in microglia modulation (38), future studies should further address a putative role of HSL in controlling neuroinflammatory cues.

The possibility of functional rather than structural derangement in synapses, as well as the low-grade inflammation, suggests that HSL is a key regulator of neuroactive lipid products. Indeed, we have identified overall basal changes in the concentration of eicosanoids and endocannabinoids induced by HSL deletion in the cortex and hippocampus. Most of these functional lipid products originate from arachidonic acid, which is a relatively abundant fatty acid in the brain produced from 2-AG and arachidonate-containing phospholipids (39). In addition to being the primary hydrolytic enzyme for 2-AG, the most abundant endocannabinoid in the brain (11), MAGL is considered to be the rate-limiting enzyme for release of arachidonic acid in the brain, to be used for the COX1/2-dependent synthesis of neuroinflammatory prostaglandins and other eicosanoids, namely prostaglandin E<sub>2</sub>, PGD<sub>2</sub>, PGF<sub>2</sub>α, and thromboxane B<sub>2</sub> (40). Although HSL has no phospholipase activity (41), these metabolites contributed to the differences observed in the profile of bioactive lipids between HSL<sup>-/-</sup> and



HSL<sup>+/+</sup> mice (Fig. 6). Thus, HSL might also have a role in the production of such eicosanoids from arachidonate-containing TAGs that are stored in lipid droplets. Interestingly, we observed reduced expression of cortical *Cox1* and hippocampal *Magl* and lower levels of PGD2 in both cortex and hippocampus of HSL<sup>-/-</sup> than HSL<sup>+/+</sup> mice. PGD2 is a known driver of neuroinflammation and affords communication from activated microglia to astrocytes (42). The reduction of PGD2 in HSL<sup>-/-</sup> mice is thus in line with low-grade neuroinflammation in the absence of gliosis (we observed no increase in levels of ionized calcium binding adapter molecule 1 and GFAP).

Eicosanoids also participate in the modulation of cerebral blood flow in response to neuronal demands by acting on the vascular bed (5, 14). Namely, both hippocampus and cortex of HSL<sup>-/-</sup> mice showed reduced levels of 20-hydroxyarachidonic acid (or 20-Hydroxyeicosatetraenoic acid), which acts as vasoconstrictor and mediates autoregulation of cerebral blood flow (43). PGF2 $\alpha$  also acts as cerebral vasoconstrictor (44) and was found increased in both cortex and hippocampus of HSL<sup>-/-</sup> mice. In the brain, the epoxyeicosatrienoic acids 5,6-EpETrE, 8,9-EpETrE, 11,12-EpETrE, and 14,15-EpETrE are locally produced to induce vessel dilation (45, 46). HSL<sup>-/-</sup> mice showed increased 5,6-EpETrE and 14,15-EpETrE in cortex and reduced 8,9-EpETrE and 11,12-EpETrE in the hippocampus. Altogether, these alterations could impact resting autoregulation as well as activity-induced neurovascular coupling. The lack of matching nutrient supply from the circulation to the demands of neuronal work is certainly critical for adequate functional performance. Cellular adaptations might be in place in HSL<sup>-/-</sup> mice to cope with the lack of vascular flexibility, and our analysis found for example the increase in expression of genes coding for PGC1 $\alpha$  that regulates mitochondria physiology, the glucose carrier GLUT1 that is ubiquitous in blood vessels and brain cells, as well as the neuronal-specific GLUT3. In contrast, there were negligible changes in insulin-sensitive GLUT4 that is strategically located near synapses for neurotransmission fueling (47), and there was a reduction in the expression of genes coding for hexokinase 1 and glycogen phosphorylase B (glycogen phosphorylase muscle isoform). These gene-expression alterations occurred in the hippocampus that controls spatial memory, and one might speculate that they could preclude that they limit glucose and glycogen metabolism during high energy demands of a memory task.

Together, MAGL, ABHD12, and ABHD6 control about 99% of 2-AG signaling in the brain (48), and each enzyme exhibits a distinct subcellular distribution, suggesting that they regulate distinct pools of 2-AG in the nervous system (7). Expression of genes coding for ABHD12 and ABHD6 was modified in cortex and hippocampus, respectively. Furthermore, *Magl* expression

tended to be increased in the cortex and reduced in the hippocampus to nearly half of that in wild-type mice. Despite small, *Magl* expression changes upon HSL deletion might still be critical in the dampening of endocannabinoid signaling in confined compartments such as the synapse, namely for removal of 2-AG produced following neurotransmitter release. Indeed, genetic deletion of MAGL results in the accumulation of 2-AG and other MAG species in the brain, without changes in expression of genes coding for HSL, ABHD6, and ABHD12 (49). None of the most studied endocannabinoids—2-AG and anandamide—were modified in the hippocampus and cortex by HSL deletion. However, it should be noted that our lipid profile was measured in the resting brain, not in response to increased neuronal activity that is the trigger for endocannabinoid synthesis and release (8).

Although no *Faah* expression changes were induced by HSL deletion, anandamide concentration was lower in the hippocampus of HSL<sup>-/-</sup> than HSL<sup>+/+</sup> mice. While increase of brain anandamide by acute inhibition of FAAH is deleterious and causes memory impairment via CB1 receptor signaling in the hippocampus (50), it can also have anti-inflammatory actions on microglia, and consequently, a neuroprotective action (51). Thus, a chronic reduction of anandamide levels in the hippocampus of HSL<sup>-/-</sup> mice can dampen its role as a gatekeeper of microglia overactivation and contribute to low-grade neuroinflammation. Furthermore, anandamide can bind to PPAR $\alpha$  and PPAR $\gamma$ , through which affords neuroprotection, anti-inflammatory effects, or metabolic regulation (52). FAAH hydrolyzes other bioactive lipids, such as POEA that was increased by HSL deletion. POEA is believed to share physiological actions with oleoylethanolamide, to which is structurally similar (53). Oleoylethanolamide shows vasorelaxation properties that contribute to controlling brain perfusion (54) and can function as endogenous ligand for cannabinoid receptors and PPAR $\alpha$  (52, 55). The alteration in the balance of anandamide and POEA is likely to impact hippocampal metabolism, including PPAR $\alpha$ / $\gamma$  regulation of mitochondrial physiology, as suggested by the observed alterations in expression of *Ppargc1a* or its isoforms in HSL<sup>-/-</sup> mice.

DAGL- $\alpha$  deletion in mice was also proposed to disrupt learning and memory because of the depletion of 2-AG and arachidonic acid across the whole brain (56). Interestingly, Schurman *et al.* (56) found effects of DAGL- $\alpha$  deletion on brain anandamide levels that were not mimicked by pharmacological inhibition of the enzyme, indicating that enzyme activities producing and/or degrading anandamide are also impacted by deletion of DAGL- $\alpha$ . In our study, we measured expression of such enzymes and found negligible effects triggered by HSL deletion.


HSL shows broad substrate specificity. Despite highest lipase activity against DAG, HSL can hydrolyze any

acylglycerol and also shows esterase activity toward cholesteryl esters, steroid fatty acid esters, or retinyl esters (41). Therefore, another possible role for HSL can be related to mobilization of cholesterol esters from lipid droplets in brain cells, which is necessary for the formation of myelin sheaths and synaptic contacts, as well as to synaptic strengthening during learning (57). Thus, we cannot exclude that the lack of a putative cholesterol esterase activity by HSL contributes to the observed memory impairment in HSL<sup>-/-</sup> mice.

A limitation of our study is the employment of a mouse model with global deletion of HSL. The HSL<sup>-/-</sup> is leaner and shows increased circulating insulin but unaltered glycemia, suggesting insulin resistance (35). While reduced fat mass could be beneficial for brain function, severe insulin resistance can contribute for memory impairment (28, 29). Brain insulin resistance in this model has hitherto not been explored.

In sum, we found no signs of substantial synaptic degeneration, astrogliosis, or microgliosis, but there was a mild increase in levels of proinflammatory cytokines. The profile of endocannabinoids and eicosanoids was distinct in the hippocampus and cortex of HSL<sup>-/-</sup> and HSL<sup>+/+</sup> mice, which might underlie the observed memory impairment. Therefore, we conclude that HSL is a key modulator of eicosanoids that are immunomodulators and further propose a role for HSL on the neuroactive and vasoactive lipid synthesis upon demand by increased neuronal activity. The later remains to be demonstrated.

#### Data availability

All data are contained within the article and can be shared upon request to J.M.N.D. (Lund University, [joao.duarte@med.lu.se](mailto:joao.duarte@med.lu.se)). 

#### Supplemental data

This article contains [supplemental data](#).

#### Acknowledgments

This work was supported by the Swedish foundation for International Cooperation in Research and Higher education (grant no.: BR2019-8508), Swedish Research Council (grant no.: 2019-01130), Diabetesfonden (grant no.: Dia2019-440), Crafoord Foundation (grant nos.: 20190007 and 20200564), Tage Blücher Foundation, Dementiafonden, and Direktör Albert Pålssons Foundation (grant nos.: FB2018-0265 and FB2019-0321). The authors acknowledge support from the Lund University Diabetes Centre, which is funded by the Swedish Research Council (Strategic Research Area EXODIAB; grant no.: 2009-1039) and the Swedish Foundation for Strategic Research (grant no.: IRC15-0067). The authors thank Dr Isak Martinsson and Prof Gunnar K. Gouras for providing the cell cultures for this study and Sara Larsson for technical assistance with the HSL activity measurements. Lund University Bioimaging Centre is acknowledged for providing access to microscopy resources. Swedish Metabolomics Centre (Umeå, Sweden) is acknowledged for the measurement of oxylipins and endocannabinoids.

#### Author contributions

C. H. and J. M. N. D. methodology; C. S., C. H., and J. M. N. D. formal analysis; C. S. and C. H. investigation; C. S., C. H., and J. M. N. D. writing–review & editing.

#### Author ORCIDs

Cecilia Skoug  <https://orcid.org/0000-0002-4999-1939>

João M.N. Duarte  <https://orcid.org/0000-0001-5984-1574>

#### Funding and additional information

J. M. N. D. acknowledges generous financial support from The Knut and Alice Wallenberg Foundation and the Faculty of Medicine at Lund University and Region Skåne.

#### Conflict of interest

The authors declare that they have no conflicts of interest with the contents of this article.

#### Abbreviations

ABHD6, alpha/beta-hydrolase domain containing 6; 2-AG, 2-arachidonoylglycerol; cDNA, complementary DNA; COX1, cyclooxygenase 1; DAG, diacylglycerol; DAGL, diacylglycerol lipase; FAAH, fatty acid amide hydrolase; GFAP, glial fibrillary acidic protein; GLUT, glucose transporter; HSL, hormone-sensitive lipase; IL, interleukin; MAGL, monoacylglycerol lipase; PGC1 $\alpha$ , PPAR gamma coactivator 1- $\alpha$ ; PGD2, prostaglandin D2; PGF2 $\alpha$ , prostaglandin F2 $\alpha$ ; PLS-DA, partial least-squares discriminant analysis; POEA, palmitoylethanolamide; SNAP25, synaptosomal-associated protein 25; TAG, triacylglycerol; VIP, variable importance in projection.

Manuscript received September 10, 2021, and in revised form February 21, 2022. Published, JLR Papers in Press, March 15, 2022, <https://doi.org/10.1016/j.jlr.2022.100195>

## REFERENCES

- Haemmerle, G., Zimmermann, R., Hayn, M., Theussl, C., Waeg, G., Wagner, E., Sattler, W., Magin, T. M., Wagner, E. F., and Zechner, R. (2002) Hormone-sensitive lipase deficiency in mice causes diglyceride accumulation in adipose tissue, muscle, and testis. *J. Biol. Chem.* **277**, 4806–4815
- Kuge, Y., Yajima, K., Kawashima, H., Yamazaki, H., Hashimoto, N., and Miyake, Y. (1995) Brain uptake and metabolism of [1-<sup>14</sup>C] octanoate in rats: pharmacokinetic basis for its application as a radiopharmaceutical for studying brain fatty acid metabolism. *Ann. Nucl. Med.* **9**, 137–142
- Ebert, D., Haller, R. G., and Walton, M. E. (2003) Energy contribution of octanoate to intact rat brain metabolism measured by <sup>13</sup>C nuclear magnetic resonance spectroscopy. *J. Neurosci.* **23**, 5928–5935
- Etschmaier, K., Becker, T., Eichmann, T. O., Schweinzer, C., Scholler, M., Tam-Amersdorfer, C., Poeckl, M., Schuligoi, R., Kober, A., Chirackal Manavalan, A. P., Rechberger, G. N., Streith, I. E., Zechner, R., Zimmermann, R., and Panzenboeck, U. (2011) Adipose triglyceride lipase affects triacylglycerol metabolism at brain barriers. *J. Neurochem.* **119**, 1016–1028
- Sonnay, S., Gruetter, R., and Duarte, J. M. N. (2017) How energy metabolism supports cerebral function: insights from <sup>13</sup>C magnetic resonance studies *in vivo*. *Front. Neurosci.* **11**, 288
- Dienel, G. A. (2019) Brain glucose metabolism: integration of energetics with function. *Physiol. Rev.* **99**, 949–1045
- Blankman, J. L., Simon, G. M., and Cravatt, B. F. (2007) A comprehensive profile of brain enzymes that hydrolyze the

- endocannabinoid 2-arachidonoylglycerol. *Chem. Biol.* **14**, 1347–1356
8. Metna-Laurent, M., and Marsicano, G. (2015) Rising stars: modulation of brain functions by astroglial type-1 cannabinoid receptors. *Glia*. **63**, 353–364
  9. Iannotti, F. A., Di Marzo, V., and Petrosino, S. (2016) Endocannabinoids and endocannabinoid-related mediators: Targets, metabolism and role in neurological disorders. *Prog. Lipid Res.* **62**, 107–128
  10. Duarte, J. M. N., Ferreira, S. G., Carvalho, R. A., Cunha, R. A., and Köfalvi, A. (2012) CB<sub>1</sub> receptor activation inhibits neuronal and astrocytic intermediary metabolism in the rat hippocampus. *Neurochem. Int.* **60**, 1–8
  11. Dinh, T. P., Carpenter, D., Leslie, F. M., Freund, T. F., Katona, I., Sensi, S. L., Kathuria, S., and Piomelli, D. (2002) Brain monoacylglyceride lipase participating in endocannabinoid inactivation. *Proc. Natl. Acad. Sci. U. S. A.* **99**, 10819–10824
  12. Cravatt, B. F., Giang, D. K., Mayfield, S. P., Boger, D. L., Lerner, R. A., and Gilula, N. B. (1996) Molecular characterization of an enzyme that degrades neuromodulatory fatty-acid amides. *Nature*. **384**, 83–87
  13. Donvito, G., Nass, S. R., Wilkerson, J. L., Curry, Z. A., Schurman, L. D., Kinsey, S. G., and Lichtman, A. H. (2018) The endogenous cannabinoid system: A budding source of targets for treating inflammatory and neuropathic pain. *Neuropsychopharmacology*. **43**, 52–79
  14. Attwell, D., Buchan, A. M., Charpak, S., Lauritzen, M., Macvicar, B. A., and Newman, E. A. (2010) Glial and neuronal control of brain blood flow. *Nature*. **468**, 232–243
  15. Kraemer, F. B., and Shen, W. J. (2002) Hormone-sensitive lipase: control of intracellular tri-(di)-acylglycerol and cholesteryl ester hydrolysis. *J. Lipid Res.* **43**, 1585–1594
  16. Mulder, H., Sorhede-Winzell, M., Contreras, J. A., Fex, M., Strom, K., Ploug, T., Galbo, H., Arner, P., Lundberg, C., Sundler, F., Ahren, B., and Holm, C. (2003) Hormone-sensitive lipase null mice exhibit signs of impaired insulin sensitivity whereas insulin secretion is intact. *J. Biol. Chem.* **278**, 36380–36388
  17. Martinsson, I., Capetillo-Zarate, E., Faideau, M., Willén, K., Esteras, N., Frykman, S., Tjernberg, L. O., and Gouras, G. K. (2019) APP depletion alters selective pre- and post-synaptic proteins. *Mol. Cell Neurosci.* **95**, 86–95
  18. Attar, A., Liu, T., Chan, W. T., Hayes, J., Nejad, M., Lei, K., and Bitan, G. (2013) A shortened Barnes maze protocol reveals memory deficits at 4-months of age in the triple-transgenic mouse model of Alzheimer's disease. *PLoS One* **8**, e80355
  19. Harrison, F. E., Reiserer, R. S., Tomarken, A. J., and McDonald, M. P. (2006) Spatial and nonspatial escape strategies in the Barnes maze. *Learn. Mem.* **13**, 809–819
  20. Duarte, J. M. N., Agostinho, P. M., Carvalho, R. A., and Cunha, R. A. (2012) Caffeine consumption prevents diabetes-induced memory impairment and synaptotoxicity in the hippocampus of NONcZNO10/LTJ mice. *PLoS One* **7**, e21899
  21. Walf, A. A., and Frye, C. A. (2007) The use of the elevated plus maze as an assay of anxiety-related behavior in rodents. *Nat. Protoc.* **2**, 322–328
  22. Mohr, A. A., Garcia-Serrano, A. M., Vieira, J. P., Skoug, C., Davidsson, H., and Duarte, J. M. N. (2021) A glucose-stimulated BOLD fMRI study of hypothalamic dysfunction in mice fed a high-fat and high-sucrose diet. *J. Cereb. Blood Flow Metab.* **41**, 1734–1743
  23. Holm, C., and Osterlund, T. (1999) Hormone-sensitive lipase and neutral cholesteryl ester lipase. *Methods Mol. Biol.* **109**, 109–121
  24. Morató, X., López-Cano, M., Canas, P. M., Cunha, R. A., and Ciruela, F. (2017) Brain membrane fractionation: An ex vivo approach to assess subsynaptic protein localization. *J. Vis. Exp.* **123**, 55661
  25. Lizarbe, B., Soares, A. F., Larsson, S., and Duarte, J. M. N. (2019) Neurochemical modifications in the hippocampus, cortex and hypothalamus of mice exposed to long-term high-fat diet. *Front. Neurosci.* **12**, 985
  26. Gouveia-Figueira, S., and Nording, M. L. (2015) Validation of a tandem mass spectrometry method using combined extraction of 37 oxylipins and 14 endocannabinoid-related compounds including prostamides from biological matrices. *Prostaglandins & Other Lipid Mediat.* **121**, 110–121
  27. Lindvall, H., Nevsten, P., Ström, K., Wallenberg, R., Sundler, F., Langin, D., Winzell, M. S., and Holm, C. (2004) A novel hormone-sensitive lipase isoform expressed in pancreatic beta-cells. *J. Biol. Chem.* **279**, 3828–3836
  28. de Bem, A. F., Krolow, R., Farias, H. R., de Rezende, V. L., Gelain, D. P., Moreira, J., Duarte, J. M. N., and de Oliveira, J. (2021) Animal models of metabolic disorders in the study of neurodegenerative diseases: An overview. *Front. Neurosci.* **14**, 604150
  29. Garcia-Serrano, A. M., and Duarte, J. M. N. (2020) Brain metabolism alterations in type 2 diabetes: What did we learn from diet-induced diabetes models? *Front. Neurosci.* **14**, 229
  30. Sekiya, M., Osuga, J., Okazaki, H., Yahagi, N., Harada, K., Shen, W. J., Tamura, Y., Tomita, S., Izuka, Y., Ohashi, K., Okazaki, M., Sata, M., Nagai, R., Fujita, T., Shimano, H., et al. (2004) Absence of hormone-sensitive lipase inhibits obesity and adipogenesis in Lep<sup>ob/ob</sup> mice. *J. Biol. Chem.* **279**, 15084–15090
  31. Hundahl, C., Kotzbeck, P., Burm, H. B., Christiansen, S. H., Torz, L., Helge, A. W., Madsen, M. P., Ratner, C., Serup, A. K., Thompson, J. J., Eichmann, T. O., Pers, T. H., Woldbye, D., Piomelli, D., Kiens, B., et al. (2021) Hypothalamic hormone-sensitive lipase regulates appetite and energy homeostasis. *Mol. Metab.* **47**, 101174
  32. Tao-Cheng, J. H., Pham, A., Yang, Y., Winters, C. A., Gallant, P. E., and Reese, T. S. (2015) Syntaxin 4 is concentrated on plasma membrane of astrocytes. *Neuroscience*. **286**, 264–271
  33. Morrison, J. H., and Baxter, M. G. (2012) The ageing cortical synapse: hallmarks and implications for cognitive decline. *Nat. Rev. Neurosci.* **13**, 240–250
  34. Sheng, M., Sabatini, B. L., and Südhof, T. C. (2012) Synapses and Alzheimer's disease. *Cold Spring Harb. Perspect. Biol.* **4**, a005777
  35. Hansson, O., Ström, K., Güner, N., Wierup, N., Sundler, F., Höglund, P., and Holm, C. (2006) Inflammatory response in white adipose tissue in the non-obese hormone-sensitive lipase null mouse model. *J. Proteome Res.* **5**, 1701–1710
  36. Fernandez, C., Schuhmann, K., Herzog, R., Fielding, B., Frayn, K., Shevchenko, A., James, P., Holm, C., and Ström, K. (2011) Altered desaturation and elongation of fatty acids in hormone-sensitive lipase null mice. *PLoS One* **6**, e21603
  37. Morigny, P., Houssier, M., Mairal, A., Ghilain, C., Mouisel, E., Benhamed, F., Masri, B., Recazes, E., Denechaud, P. D., Tavernier, G., Caspar-Bauguil, S., Virtue, S., Sramkova, V., Monbrun, L., Mazars, A., et al. (2019) Interaction between hormone-sensitive lipase and ChREBP in fat cells controls insulin sensitivity. *Nat. Metab.* **1**, 133–146
  38. Layé, S., Nadjar, A., Joffre, C., and Bazinet, R. P. (2018) Anti-inflammatory effects of omega-3 fatty acids in the brain: Physiological mechanisms and relevance to pharmacology. *Pharmacol. Rev.* **70**, 12–38
  39. Contreras, M. A., Greiner, R. S., Chang, M. C., Myers, C. S., Salem, N., Jr., and Rapoport, S. I. (2000) Nutritional deprivation of alpha-linolenic acid decreases but does not abolish turnover and availability of unacylated docosahexaenoic acid and docosahexaenoyl-CoA in rat brain. *J. Neurochem.* **75**, 2392–2400
  40. Nomura, D. K., Morrison, B. E., Blankman, J. L., Long, J. Z., Kinsey, S. G., Marcondes, M. C., Ward, A. M., Hahn, Y. K., Lichtman, A. H., Conti, B., and Cravatt, B. F. (2011) Endocannabinoid hydrolysis generates brain prostaglandins that promote neuroinflammation. *Science*. **334**, 809–813
  41. Holm, C., Osterlund, T., Laurell, H., and Contreras, J. A. (2000) Molecular mechanisms regulating hormone-sensitive lipase and lipolysis. *Annu. Rev. Nutr.* **20**, 365–393
  42. Mohri, I., Taniike, M., Taniguchi, H., Kanekiyo, T., Aritake, K., Inui, T., Fukumoto, N., Eguchi, N., Kushi, A., Sasai, H., Kanaoka, Y., Ozono, K., Narumiya, S., Suzuki, K., and Urade, Y. (2006) Prostaglandin D<sub>2</sub>-mediated microglia/astrocyte interaction enhances astrogliosis and demyelination in twitcher. *J. Neurosci.* **26**, 4383–4393
  43. Harder, D. R., Narayanan, J., and Gebremedhin, D. (2011) Pressure-induced myogenic tone and role of 20-HETE in mediating autoregulation of cerebral blood flow. *Am. J. Physiol. Heart Circ. Physiol.* **300**, H1557–H1565
  44. Salom, J. B., Torregrosa, G., Miranda, F. J., Alabadi, J. A., Alvarez, C., and Alborch, E. (1991) Ca<sup>2+</sup> entry blockers inhibit prostaglandin F<sub>2</sub> alpha-induced cerebrovascular contractile responses in goats. *Eur. J. Pharmacol.* **203**, 33–39
  45. Gebremedhin, D., Ma, Y. H., Falck, J. R., Roman, R. J., VanRollins, M., and Harder, D. R. (1992) Mechanism of action of cerebral epoxyeicosatrienoic acids on cerebral arterial smooth muscle. *Am. J. Physiol.* **263**, H519–H525



46. Alkayed, N. J., Narayanan, J., Gebremedhin, D., Medhora, M., Roman, R. J., and Harder, D. R. (1996) Molecular characterization of an arachidonic acid epoxygenase in rat brain astrocytes. *Stroke* **27**, 971–979
47. Ashrafi, G., Wu, Z., Farrell, R. J., and Ryan, T. A. (2017) GLUT4 mobilization supports energetic demands of active synapses. *Neuron* **93**, 606–615.e3
48. Savinainen, J. R., Saario, S. M., and Laitinen, J. T. (2012) The serine hydrolases MAGL, ABHD6 and ABHD12 as guardians of 2-arachidonoylglycerol signalling through cannabinoid receptors. *Acta Physiol* **204**, 267–276
49. Taschler, U., Radner, F. P., Heier, C., Schreiber, R., Schweiger, M., Schoiswohl, G., Preiss-Landl, K., Jaeger, D., Reiter, B., Koefeler, H. C., Wojciechowski, J., Theussl, C., Penninger, J. M., Lass, A., Haemmerle, G., et al. (2011) Monoglyceride lipase deficiency in mice impairs lipolysis and attenuates diet-induced insulin resistance. *J. Biol. Chem.* **286**, 17467–17477
50. Basavarajappa, B. S., Nagre, N. N., Xie, S., and Subbanna, S. (2014) Elevation of endogenous anandamide impairs LTP, learning, and memory through CB1 receptor signaling in mice. *Hippocampus* **24**, 808–818
51. Eljaschewitsch, E., Witting, A., Mawrin, C., Lee, T., Schmidt, P. M., Wolf, S., Hoertnagl, H., Raine, C. S., Schneider-Stock, R., Nitsch, R., and Ullrich, O. (2006) The endocannabinoid anandamide protects neurons during CNS inflammation by induction of MKP-1 in microglial cells. *Neuron* **49**, 67–79
52. O'Sullivan, S. E. (2016) An update on PPAR activation by cannabinoids. *Br. J. Pharmacol.* **173**, 1899–1910
53. Tovar, R., Gavito, A. L., Vargas, A., Soverchia, L., Hernandez-Folgado, L., Jagerovic, N., Baixeras, E., Ciccocioppo, R., Rodriguez de Fonseca, F., and Decara, J. (2021) Palmitoleylethanolamide is an efficient anti-obesity endogenous compound: comparison with oleylethanolamide in diet-induced obesity. *Nutrients* **13**, 2589
54. Wheal, A. J., Alexander, S. P., and Randall, M. D. (2010) Vaso-relaxation to *N*-oleylethanolamine in rat isolated arteries: mechanisms of action and modulation via cyclooxygenase activity. *Br. J. Pharmacol.* **160**, 701–711
55. Fu, J., Gaetani, S., Oveisi, F., Lo Verme, J., Serrano, A., Rodriguez De Fonseca, F., Rosengarth, A., Luecke, H., Di Giacomo, B., Tarzia, G., and Piomelli, D. (2003) Oleylethanolamide regulates feeding and body weight through activation of the nuclear receptor PPAR- $\alpha$ . *Nature* **425**, 90–93
56. Schurman, L. D., Carper, M. C., Moncayo, L. V., Ogasawara, D., Richardson, K., Yu, L., Liu, X., Poklis, J. L., Liu, Q. S., Cravatt, B. F., and Lichtman, A. H. (2019) Diacylglycerol lipase- $\alpha$  regulates hippocampal-dependent learning and memory processes in mice. *J. Neurosci.* **39**, 5949–5965
57. Petrov, A. M., Kasimov, M. R., and Zefirov, A. L. (2016) Brain cholesterol metabolism and its defects: Linkage to neurodegenerative diseases and synaptic dysfunction. *Acta naturae* **8**, 58–73